Proceedings World Geothermal Congress 2020+1
Reykjavik, Iceland, April - October 2021

Imaging the 2010-2011 Inflationary Source at Krysuvik, SW Iceland, Using Time-Dependent Vp/Vs Tomography

Alex Hobé, Olafur Gudmundsson, Ari Tryggvason, SIL seismological group

Villavägen 16, 75236 Uppsala, Sweden

alex.hobe@geo.uu.se

Keywords: Vp/Vs tomography, time-dependent seismic tomography, Krysuvik, geothermal energy, surface deformation

ABSTRACT

Near Reykjavik, the capital of Iceland, lies the Krysuvik high-temperature geothermal area, which could potentially provide vast amounts of energy to this and surrounding towns and villages. Possible changes to the heat-source and/or hydrothermal system in this area are indicated by a period of surface deformation between 2007 and 2016 (Gudjonsdottir et al., 2018). This study provides subsurface images below Krysuvik and the neighboring areas with high resolution down to 10 km depth using 15 years of earthquake data. These images indicate regions of partial-melt and a large super-critical reservoir below ~5 km depth, which would serve well as a fluid source for a new power-plant. The robustness of this model is assessed using time-dependent seismic tomography. Through systematic study of known issues with time-dependent seismic tomography, it is shown that significant changes do occur in the results on time-scales comparable to the surface deformation. Changes that we assess and suggest are significant beyond e.g. the influence of differences in ray-path geometries and travel-time errors. Several hypotheses are developed based on these results and available information from multiple disciplines. Based on this integration of information with our results, the most likely explanations of the surface deformation signal are: 1) strong degassing of a magmatic source due to increased heat from deeper magmatic infiltration, and 2) bending and subsequent fracturing of an impermeable barrier by expanding fluids.

1. INTRODUCTION

The Krysuvik high-temperature geothermal area is located on the Reykjanes Peninsula in south-west Iceland.A possible exploitation of the system may be interrelated with the feasibility of developing IceLink (Sasaki and Nakayama, 2016), a ~1 GW transmission link between Iceland and the UK. IceLink would break the isolation of the Icelandic electricity system and open up new markets for suppliers in both countries. The project may be commenced in the late 20's and complete in five to six years. The project is economically feasible as the UK seeks to reduce its reliance on fossil fuels and needs economical solution balancing an electric system with a high penetration of intermittent generation. A possible development of the Krysuvik geothermal system is interesting in this context. Understanding the details of the heat source and the hydrothermal system is vital for assessing the potential of the geothermal resource and the risks associated with its exploitation. Between 2007 and 2016, the Krysuvik area went through a prolonged period of surface deformation (Gudjonsdottir et al., 2018). The fastest inflation (8 cm in two years) occurred between March of 2010 and January of 2012. This period of rapid inflation was followed by a slower deflation period (~1.7 cm/year), which still continues (Hreinsdottir and Michalczewska, 2019).

These observations suggest that changes occurred to the heat-source and/or the hydrothermal system of this geothermal area. Changes that might be observed with time-dependent seismic tomography. However, simply inverting data from different time-periods independently and expecting robust information about temporal variations in the subsurface may be misleading. Several issues can arise when using travel-times from natural earthquakes from different time-periods (e.g. Julian and Foulger 2010). When the same forward solver is used, these are: 1) temporal differences in earthquake distributions, 2) temporal differences in station geometries, 3) errors in the arrival times, and 4) the impact of regularization when using different numbers of earthquakes and P- and S-wave travel-times. Issues 1) and 2) can introduce a bias in the results due to differences in ray-path geometries. The random component of issue 3) we suggest is less of a problem when using quality data, but there may be systematic errors (biases) that may introduce artifacts in the resulting models. Issue 4) may dampen or smooth out features when there are less data available that sample them. These issues make it difficult to distinguish true temporal variations in the subsurface from artificial changes. Multiple authors have made contributions to the quest for robustness in time-dependent seismic tomography (e.g. Julian and Foulger, 2010; Koulakov et al., 2013). At least two ways have been used to mitigate the effects of these issues on the interpretation of tomographic changes with time: 1) producing appraisal information (e.g. synthetic models and checkerboard tests) that is taken into account during interpretation (e.g. Koulakov et al., 2013), and 2) minimizing the differences between models inverted for simultaneously from different datasets (e.g. Julian and Foulger 2010). Neither strategy directly addresses the issues with variations in ray-path geometry and data quality. For the Krysuvik area, the long-term implementation of the South Iceland Lowlands network (SIL) assures a consistent station geometry. The area shows recurring earthquake distributions, including earthquake swarms, which greatly reduce the influence of ray-path geometry differences due to differences in earthquake location, compared to e.g. Koulakov et al., (2013), as we will show.

First and foremost, this study provides a high resolution Vp, Vs, and Vp/Vs tomography using 15 years of SIL-catalog events (2004-2018), extending below 10 km depth. This "Baseline" model is used in a time-dependent investigation to test the null-hypothesis, i.e. that no changes occur throughout the 15-year period. This has multiple benefits: 1) The Baseline model should be the closest approximation to the time-invariant signal in the data and thus provides the closest indication of velocity changes due to ray-path geometry differences. 2) Robustness of individual features in the Baseline model are tested using specific subsets of the data. This lends credence to these features and aids in interpretation. 3) If changes are insignificant in the time-period, the robust features of the Baseline model become the best current estimate. 4) If changes are significant, the Baseline model aids in interpreting these changes. The results of this investigation are discussed in light of the observed surface deformation, along with other indications from literature.

1.1 The Dataset and 1D Starting Model

Fig. 1 shows the 12 permanent SIL-stations on the Reykjanes Peninsula. 11 of these stations have been active from 2004 up to the present day, and a 12th permanent station (RNE) was introduced in 2008. Although denser networks have been implemented on the Reykjanes Peninsula during this time-period, this initial investigation focuses on data from these stations to ensure a constant station geometry. During the time-period of 2004-2018, 59 761 high quality events were detected and hand-picked. This resulted in 345 943 and 363 863 travel-times for P- and S-waves, respectively. The earthquake locations contained in the SIL-catalog were used as initial locations for the Baseline inversion. The center of the radial uplift signature (2010-2011) occurred around 22 km distance in the red profile (Fig. 1) and had a diameter of ~8 km (Michalczewska et al., 2012a). Table 1 shows the employed 1D velocity model. Its values are interpolated in between the specified values. The S-wave velocities are obtained using a Vp/Vs ratio of 1.78, which provides a good initial fit to the data and is consistent with literature (e.g. Weir et al., 2001; Tryggvason et al., 2002).

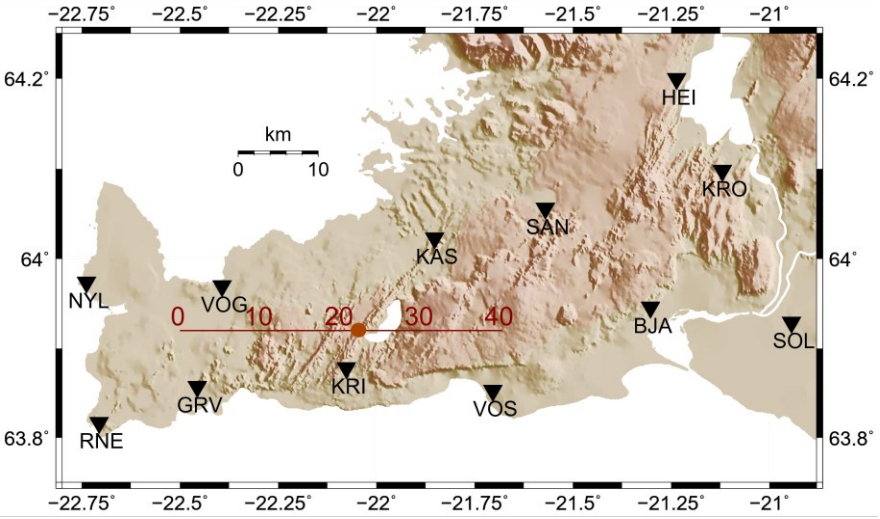

Figure 1: Map of the study area with 12 SIL stations (black triangles), profile line (red), and inflation center (orange dot).

Table 1: 1D velocity model

Depth [km]:	0	1	2	3	4	5	6	9	13	18
Vp [km/s]:	3.45	4.55	5.45	5.95	6.25	6.35	6.45	6.82	7.50	7.50

1.2 The Krysuvik Geothermal Area

The Krysuvik geothermal area is located on the trans-tensional plate boundary cutting through the Reykjanes Peninsula (e.g. Einarsson, 2008), together with multiple other volcanic systems, e.g. Fagradalsfjall to the west and Brennisteinsfjöll to the east. The profile in Fig. 1 extends beyond the Krysuvik area and crosses these neighboring volcanic systems. The most important feature of the Krysuvik geothermal area is a fissure swarm, which lies approximately perpendicular to the spreading direction. This volcanic feature is typical of the volcanic systems on the Peninsula. It is tens of km long and several km wide (Hersir et al., 2018). Its surface expression is a linear feature extending between the KRI and KAS stations (Fig. 1). There are also NS trending strike-slip faults in the Krysuvik and surrounding areas with sizes comparable to the dimensions of the Kleifarvatn lake in Fig. 1 (east of the orange dot). These strike-slip faults are an extension of the bookshelf tectonics of the southern-Iceland low-land transform, connecting the Reykjanes oblique rift to the eastern volcanic zone. The typical lithological composition of the Reykjanes Peninsula obtained from boreholes and interpolated/extrapolated with geophysical methods is as follows (see e.g. Fig. 4 in Fridleifsson and Elders, 2017; Flovenz and Gunnarson, 1991). Starting at the surface there is a zone of hyaloclastites (and some marine sediments at the Peninsula's western tip) in different stages of alteration. At ~2 km depth are pillow basalts, though this depth varies along the peninsula. Below this a complex of sheeted dikes is encountered with increasing density of intrusions with depth. The gabbroic lower crust is expected between 6 and 7 km at the Peninsula's western tip. This depth also varies along the Peninsula and is expected to increase towards the east. Between 1997 and 2006, the Krysuvik area was the most seismically active area on the Reykjanes Peninsula followed by the neighboring Fagradalsfjall, with both areas supporting recurring swarm activities (Keiding et al, 2009). Keiding et al. (2009) suggest plate motion as the primary driver of seismicity in these areas, with Krysuvik's earthquakes having geothermal fluids as a secondary trigger. This is unlikely in Fagradalsfjall, which does not have geothermal surface activity.

The deepest borehole in the area is the recent IDDP-2 well drilled in the nearby Reykjanes geothermal field (Fridleifsson and Elders, 2017). This well encountered a supercritical-fluid reservoir at 4.5 km depth, which gives further credence to the presence of dual-fluid reservoirs in the brittle crust. This hypothesis was built upon by Geoffroy and Dorbath (2008) in relation with the Kleifarvatn Lake draining by 12 vol-% over an 18-month period starting in 2000, after a magnitude ?? event. Hersir et al., 2018 investigated the subsurface resistivity in Krysuvik and related the resistivity in their model to the clay content and temperature data from the boreholes in the area. Their study found a ~70 Ωm body at 4-5 km depth correlated with the depth of the inflation source.

The crustal deformation itself was investigated by Gudjonsdottir et al. (2018), and related to the local seismicity and the gas species exiting three geothermal hot spots in the area. These gas measurements were taken ~1.5 years after subsidence had already set in. The authors suggest that periods of increased seismicity and surface deformation lead to increased fumarole activity in two ways: 1) through (temporary) new pathways and 2) increased boiling in the system. They find no evidence for increased magmatic gas contribution and evidence of a stable heat source with no increase in temperatures. The observed SO_2 species (not previously observed in the area) could also have rapidly made its way from a magmatic source using seismically created pathways.

2. METHODS

This study employed PStomo_eq (Tryggvason et al., 2002) to produce the presented tomographic inversions. PStomo_eq solves jointly for hypocentral parameters and three-dimensional P- and S-wave models. The forward travel-times are computed using a first order eikonal solver (Podvin & Lecomte, 1991; Tryggvason and Bergman, 2006). The rays needed to distribute the velocity perturbations are obtained by tracing in the time fields from the sources back towards the receivers perpendicular to the isochrons (Hole 1992; Benz et al., 1996). The inverse problem is solved by the conjugate gradient solver LSQR (Page and Saunders, 1982). Several forms of model regularization can be applied to impede wild velocity variation. Models can be required to be smoothed by the means of penalizing large values of the Laplacian of the perturbation field, and the models can be required to provide a "reasonable" Vp/Vs ratio by penalizing deviations from a "normal" value. The cross-gradients function of the P- and S-wave model can also be minimized (Tryggvason and Linde, 2006). The latter is a way to push the models towards "structural similarity" (Gallardo and Meju, 2004). As travel-time tomography is non linear (the ray paths depend on the velocity field, which is inverted for), the problem is solved iteratively with new ray-paths computed at every iteration. A commonly used strategy is to employ larger weights on the regularization during the initial iterations, compared to the final iterations. The purpose of this is to get the longer wavelength velocity variations in place, before allowing finer details into the velocity models. After the initial iterations, the earthquake locations are normally fairly well established and the ray paths deviate less between iterations, which is the motivation behind this strategy. The regularization strategy for each presented inversion is equivalent, with the final iterations having the same choice of smoothing as the only applied regularization (similar to e.g Koulakov et al., 2013).

2.1 The Trade-Off Between Temporal and Spatial Resolution

Although the seismicity in the Krysuvik and surrounding areas has a characteristic spatial distribution (see Fig. 8 in the Results Section), the temporal distribution of the seismicity patterns varies substantially. Some years have little seismicity and others have large swarms occurring within a short period. Consequently, there is an inherent trade-off between temporal and spatial resolution for seismic tomography in this area. The resolution in space is increased when using a larger time-window. This, because it includes more earthquakes in more diverse locations due to this variation in the seismicity. Assuming that temporal velocity changes occur, each inversion produces some sort of weighted average of the seismic velocities during a given time period. Longer time windows make it harder to discern these changes, if they are not constant nor incremental between the chosen time periods. To resolve any changes in the subsurface, the time window therefore needs to be small enough compared to the time in which the changes occur. At the same time, the time window needs to be large enough to resolve features comparable to the size of the subsurface change. We investigate this trade off between temporal and spatial resolution by comparing the full 15-year dataset inversion (the Baseline model) with inversions of time periods of 1, 2, 3, 4, and 5-year datasets, and with corresponding checkerboard tests. This comparison is performed for two initial models to further assess the robustness of individual features: the 1D initial model and a model based on the Baseline model. As the Baseline model is quite heterogeneous, an average model which we call "fullStart" is used to avoid complications when inverting smaller datasets. The fullStart model (Fig. 9) is obtained in the following manner. The Vp-part of the fullStart model is obtained by averaging the Baseline Vp result and the Baseline Vs result multiplied by the regional Vp/Vs ratio (1.78). The Vs-part of the fullStart model is then obtained by dividing this Vp-part of the fullStart model through by 1.78. This additionally ensures that the initial Vp/Vs ratio is 1.78 everywhere. The inversions with the 1D initial model use the locations and origin times from the SIL-catalog, whereas the fullStart inversions use the final locations and origin times of the Baseline model.

2.2 Reconstructing the Baseline Model

While checkerboard tests using the 1D starting model investigate the spatial resolution, checkerboard tests using the fullStart initial model show the ability of an inversion to spatially resolve changes away from the fullStart model. Reconstruction tests were performed to check the ability of individual datasets to reproduce the Baseline model. Thus emphasizing artificial differences from this model. The final locations and origin times obtained in the Baseline inversion were used as initial values in these reconstructions. From those values, these tests produce synthetic travel-times in the exact amount and on the same stations as available for each earthquake. Though this is standard practice in checkerboard tests, it is an important point in this study, as we are interested in the effects of ray-path geometries. Errors are then added to these synthetic travel-times, as well as to the initial earthquake locations and origin time. The inversion process is carried out equivalently to all other inversions. The origin times and earthquake locations were given errors with a standard deviation of 0.1 s, and 0.5 km horizontally and 1 km vertically, respectively. Standard deviations of 0, 10, 30, and 47 ms (for P and multiplied by 1.78 for S) were investigated for the travel-time errors.

3. RESULTS

All Figs. in this Section show the vertical profile corresponding to the red line in Fig. 1 and are arranged as follows. First, the Baseline inversion together with the checkerboard test are presented (Fig. 2). Figs. 3 and 4 show the investigation into the temporal resolution using real data with time windows increasing from single year up to 5 years. Figs. 5 and 6 show the corresponding investigation into the spatial resolution. Fig. 7 presents the checkerboard test for 2-year datasets starting from the fullStart model, indicating the ability of these inversions to show changes from this starting model. Fig. 8 shows the corresponding inversions using real data. The apparent change in time seen in Fig. 8 is further put into perspective using Figs. 9-12. Fig. 9 shows the fullStart model, as well as two reconstructions of the Baseline model using 2008-2009 data (without tt-errors and the highest chosen tt-errors). The 1st reconstruction (no tt-errors) is used as a reference in Fig. 10, which compares the results of these reconstructions between the 2-year datasets. This same comparison is repeated in Fig. 11 using the differences between the results in Fig. 8, and in Fig. 12 using the reconstructions with the largest tt-errors. All results use an equidistant parameterization of 1x1x0.5 km.

3.1 The Baseline Inversion

Fig. 2 shows the results using the full dataset spanning 15 years (the Baseline model). Included are the seismicity and the checkerboard test using 5 km wide (horizontally) and 2.5 km deep checkers. The resolution of this model is very good between 8 and 33 km distance with checkers resolved down to depths of 10 km. Vs does a little poorer near the surface, though it is able to resolve the vertical boundary between checkers at ~18 and 23 km distance.

As expected, the Baseline model shows a strong gradient near the surface in both Vp and Vs. At 2 km depth, an undulating surface (white) marks the transition to a more heterogeneous layer. The most striking feature in this layer lies directly below the approximate center of inflation (the arrow). It is a low-velocity zone between ~4.5 and 8 km depth for Vs and between ~4.5 and 10 km depth for Vp. This feature is more symmetrical for Vs, whereas it dips towards the east for Vp. Above ~30 km distance there are relatively higher velocities in this layer for both Vp and Vs. Between ~8 km and ~18 km distance and 6 and 10 km depth there is a smaller low-velocity zone for Vp. Whereas Vs has another low-velocity zone between ~4.5 and 7 km depth, up to ~5 km distance.

The Vp/Vs result shows strongly decreased and some elevated values compared to the regional average (1.78). There is a high Vp/Vs anomaly at ~18 km distance between ~3-7 km depth. Another small high Vp/Vs anomaly is found underneath (~9 km depth). Both anomalies lie in regions with strongly decreased seismicity. Adjacent to these anomalies are two larger low Vp/Vs anomalies, which span the profile vertically. The connection at ~14 km distance is associated with seismicity, and the connection at ~28 km distance does not have any seismicity associated with it above 5 km depth. At ~10 km distance the seismicity is associated with an average Vp/Vs region above 7 km depth. Towards the west of this, the seismicity decreases greatly. There, the top four kms show a low Vp/Vs region above a region with elevated Vp/Vs values. The seismicity also decreases above ~30 km distance, except below ~6 km depth. A low Vp/Vs region at these depths is overlain by a high Vp/Vs anomaly. The bottom of the overall seismicity seems to follow the upper parts of both the low Vp and low Vp/Vs structures, though some of the seismicity does lie inside.

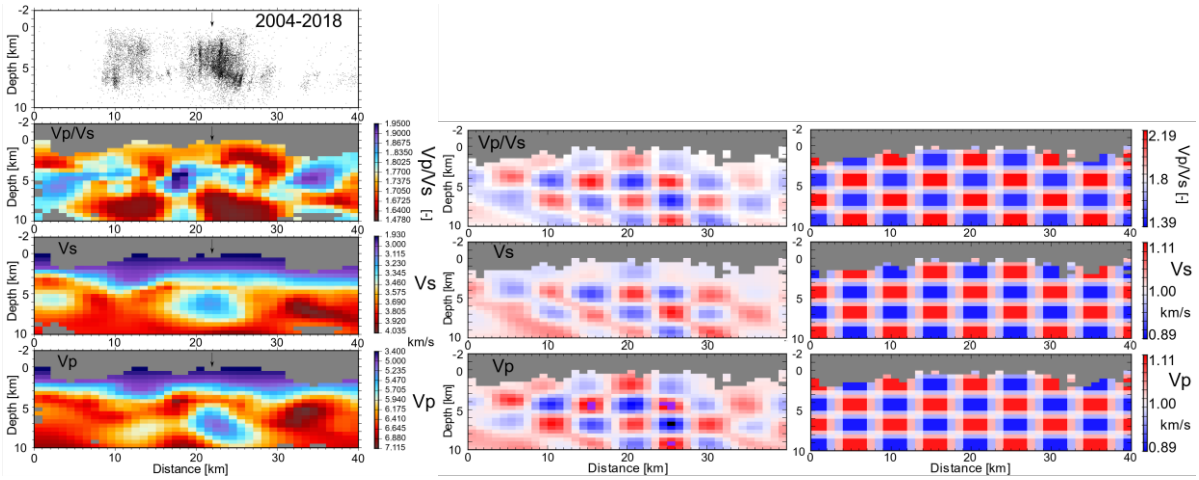

Figure 2: Left) Baseline model obtained using the full 15-year dataset starting from the 1D velocity model. The arrows indicate the approximate center of inflation at the surface. The projected seismicity lies within +/- 1.5 km distance. Middle) Corresponding checkerboard test. Right) Original checkers (Vp and Vs relative to initial 1D model).

3.1 The Trade-Off Between Temporal and Spatial Resolution

The results for the temporal resolution tests are shown in Figs. 3 and 4 using the 1D and fullStart initial models, respectively. The main features in these images are very similar, especially using 2-5 year time-windows. The following is found when comparing between the Baseline model (Fig. 2), the 1D initial model results, and those using the fullStart model: 1) There is less undulation of the white layer for the 1D case. In contrast, the fullStart case shows an undulation of this layer similar to the Baseline model for all time-windows. 2) The low Vp and Vs anomalies below the inflation center become clearer with increasing time-windows for 1D. They have a lower amplitude, compared to the Baseline, even for the 5 year time window. In the fullStart results these anomalies show strong similarities to those in the Baseline model. 3) The ray coverage increases with increasing time windows, especially at depth. Cells with no ray coverage are masked with gray colour in all Figs. 4) The Vp/Vs results show strong similarities for both the 1D and fullStart cases, though the 1D case has higher amplitudes. All Vp/Vs results for these two cases show striking differences to the Vp/Vs result of the Baseline model (e.g. the low-Vp/Vs anomaly at ~14 km distance is now a Vp/Vs high above 4.5 km depth).

Figs. 5 and 6 show the corresponding checkerboard tests using the 1D and fullStart initial models, respectively. The checkers are 5x5x2.5 km (like in Fig. 2). Although tests with larger checkers where performed, these Figs. were chosen to best illustrate the improvement (or lack thereof) of these tests with increasing time windows. Both Figs. show incremental improvement of the results. The checkerboards in Fig. 6 are slightly less well resolved compared to Fig. 5, except for a few individual checkers that are better resolved (e.g. the red checker centered on 4 km depth, 15 km distance). Fig. 7 shows similar checkerboard tests (8x8x4 km) for inversions using the fullStart initial model and 2-year time-windows. These results thus test the ability of these datasets to show changes from the fullStart model. The results are shifted by a year with respect to each other. This Fig. was chosen for the following reasons: 1) Most results resolve these checkers well, 2) The borders of the red checker between 20 and 28 km distance and below 6 km depth cut the low Vp/Vs anomaly in Fig. 4 in half with depth, and 3) It indicates the ability to make a strong horizontal separation towards the west and east. The reason for this choice will become evident when discussing Fig. 8. Between 2010-2011 and 2013-2014 there is less ray coverage at depth towards the west, compared to the other periods. The amplitude of the checkers is mostly maintained. Some checkers even slightly overshoot the original values (black for too low and purple for too high).

3.2 Apparent Changes with Time

Fig. 8 shows the inversion results using the fullStart initial model for 2-year time windows from 2008 up to 2018. It also shows how the characteristic spatial distribution of the seismicity seen in Fig. 2 is sampled over time. The stronger seismicity throughout 2008 up to the beginning of 2012 is followed by a quieter period up to the middle of 2015. This activity becomes moderately stronger again after. The seismicity domes up in the center of the profile and there seems to be a radial pattern of straight lines in the seismicity above this dome (best seen in 2010-2011). The main features in the Vp and Vs results remain stabile.

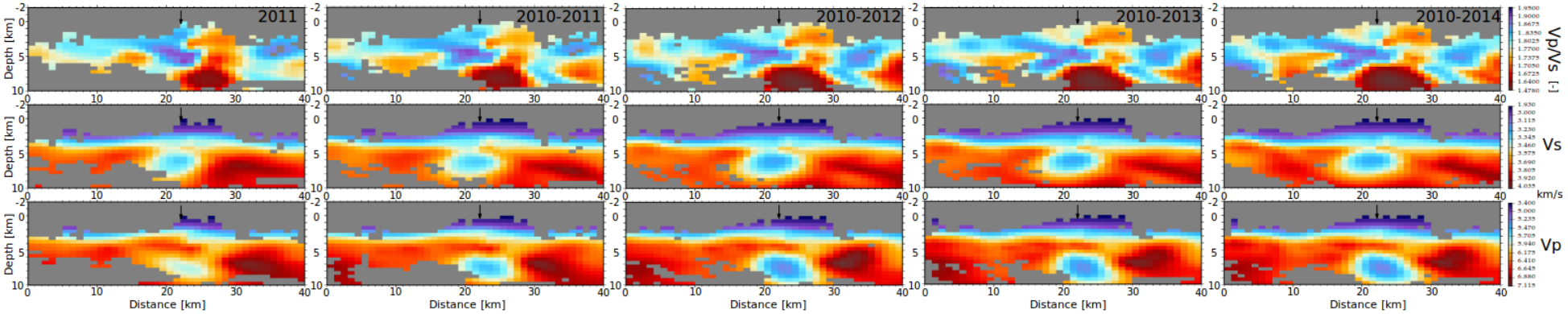

Figure 3: Temporal resolution test using 1D initial model and increasing time-window size.

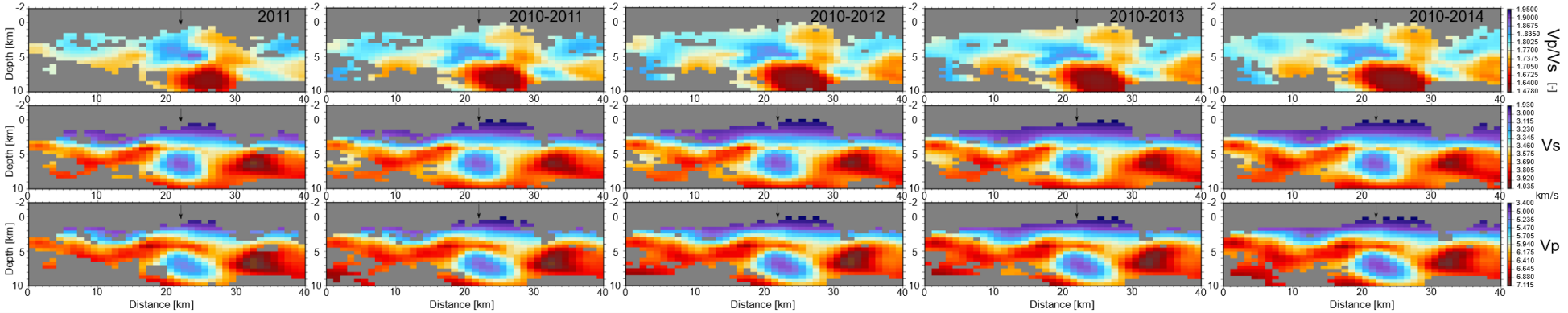

Figure 4: Temporal resolution test using fullStart initial model and increasing time-window size.

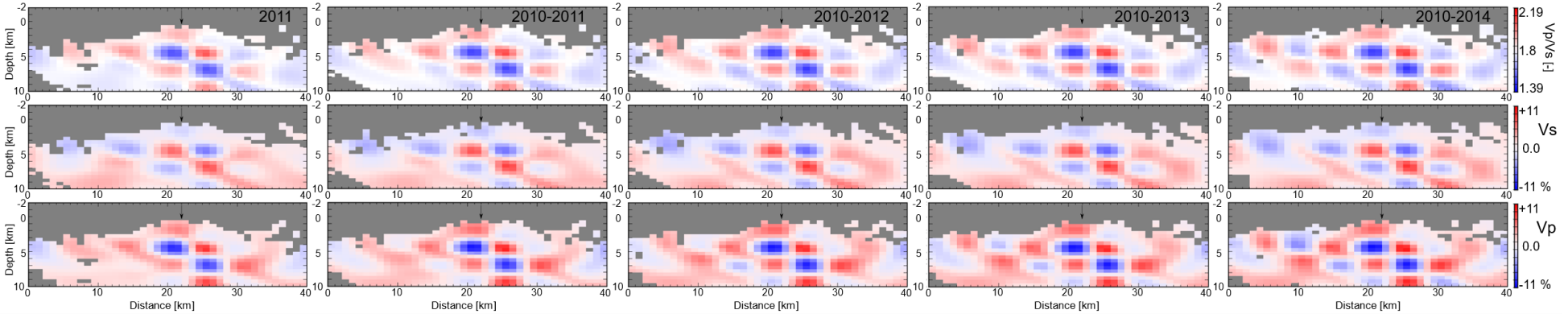

Figure 5: Checkerboard test using 1D initial model and increasing time-window size. Checkerboards are 5 km horizontally and 2.5 km with depth.

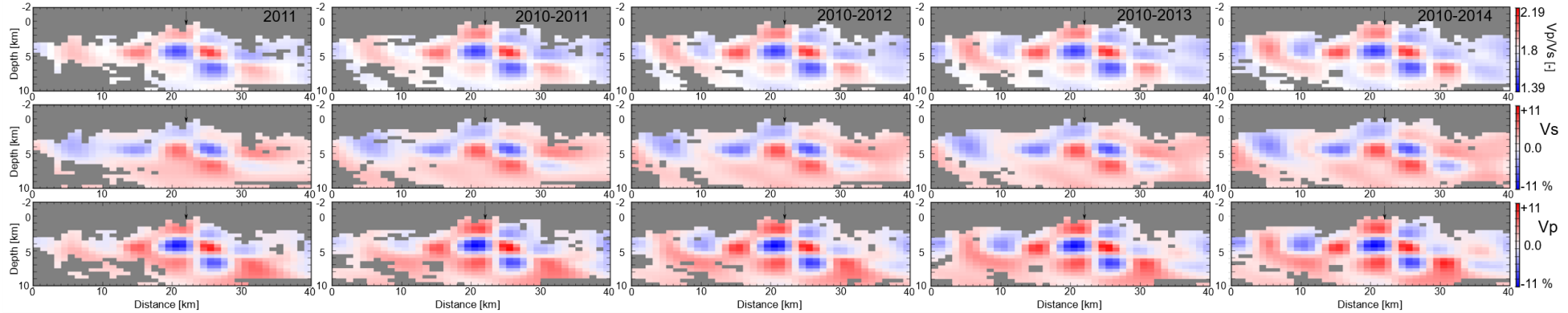

Figure 6: Checkerboard test using fullStart initial model and increasing time-window size. Checkerboards are 5 km horizontally and 2.5 km with depth.

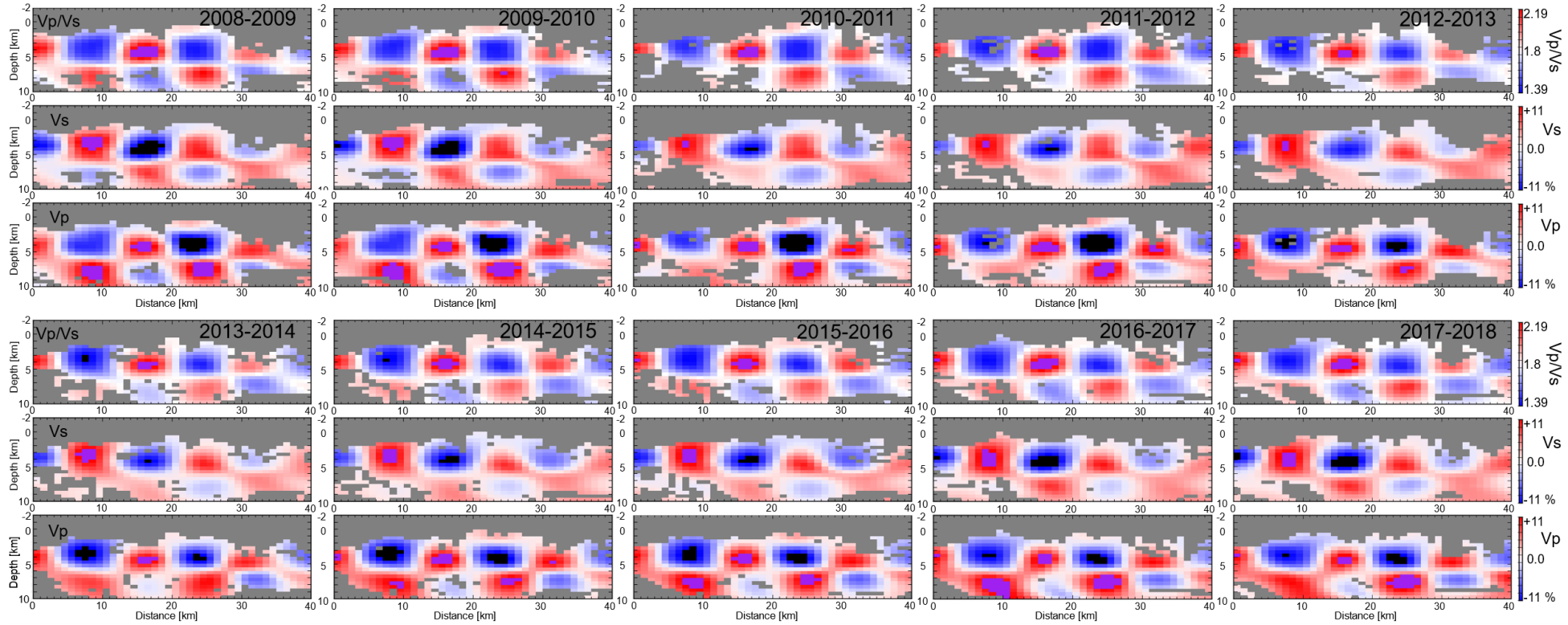

Figure 7: Checkerboard tests for models using 2-year datasets. Vp and Vs velocities are normalized to the fullStart velocity model. Vp/Vs shows the actual Vp/Vs ratio for these tests. Checkerboards are 8 km horizontally and 4 km with depth.

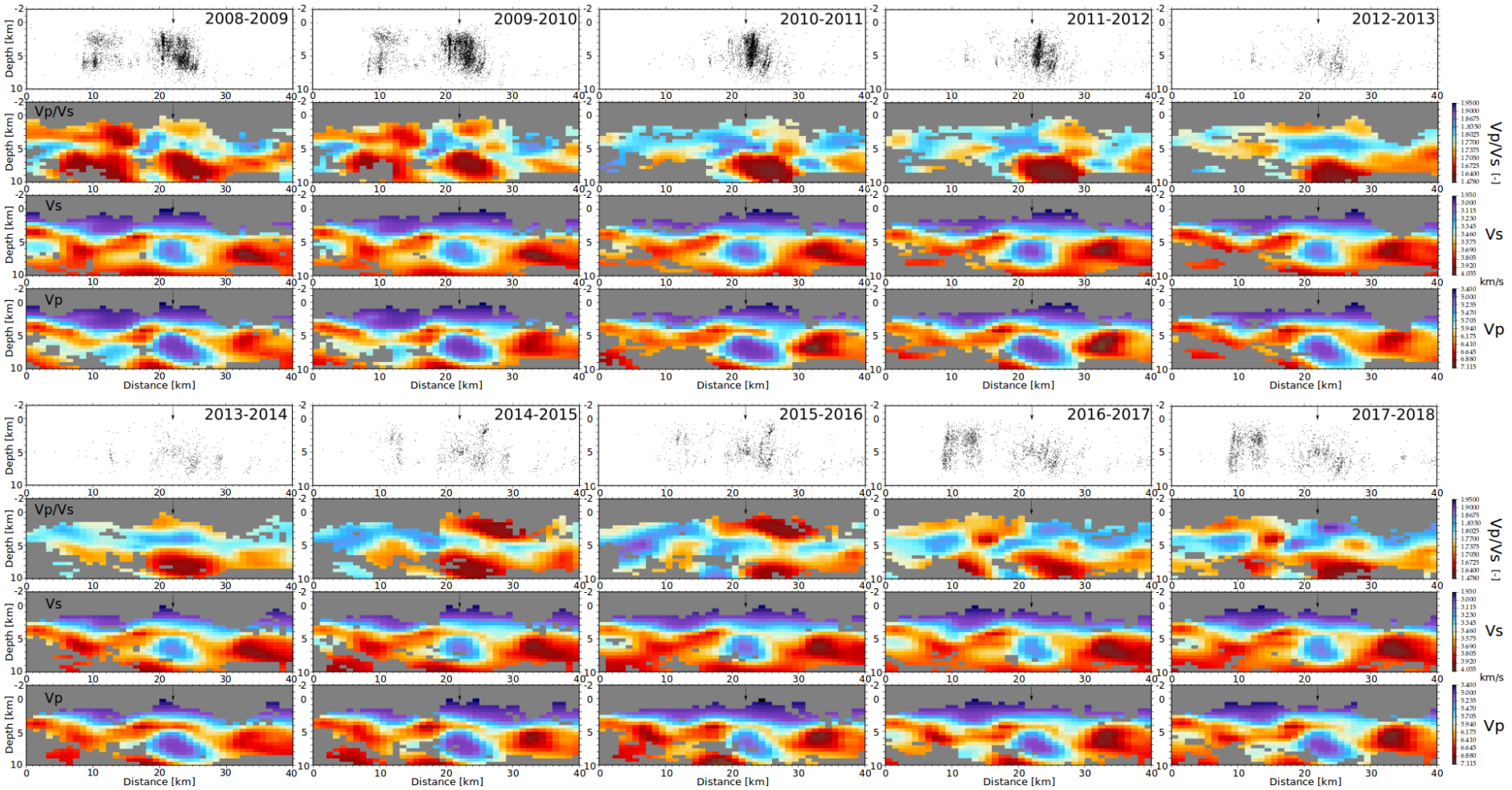

Figure 8: Results for the inversions using the fullStart initial model and 2-year time-windows. For each time-period the following are shown from top to bottom: Seismicity pattern, Vp/Vs ratio, Vs velocities, and Vp velocities. The seismicity shows all earthquakes within +/- 1.5 km of the profile in the N-S direction.

The biggest changes occur in the amplitude of the low Vp and Vs anomalies between 10 and 30 km distance between the periods 2008-2009 and 2009-2010, and the periods 2015-2016 through to 2017-2018. Striking differences occur between the panels for the Vp/Vs results. For 2008-2009, there is a Vp/Vs low centered around ~12 km distance which decreases in amplitude in 2009-2010 and reduces to a Vp/Vs average near the surface for most other panels. The exceptions being 2012-2013, 2016-2017, and 2017-2018 where this Vp/Vs low again reaches the coverage limit near the surface. The 2nd Vp/Vs low in Fig. 2 (~20-30 km distance) does not span the entire depth in the 2008-2009 result, increases in strength up to 2011-2012, and is spread east in all other panels, while being spread to the west in most results. This anomaly only connects to the surface (~26 km distance) between 2009-2010 and 2011-2012. In this same location between 2012-2013 and 2015-2016, average to high Vp/Vs values between 3-6 km depth separate a Vp/Vs low at the surface from a low at depth. In the last two time windows, the low at the surface changes to a Vp/Vs high instead. Most time-windows show a Vp/Vs high centered around 20 km distance at depths above 5 km. The amplitude of this anomaly also increases from 2008-2009 up to 2011-2012. Between 2012-2013 and 2015-2016, this anomaly diminishes in amplitude whilst forming an extended band. This band is then separated by the low Vp/Vs anomaly connecting to the surface at ~14 km distance in the last two time-windows.

3.3 Reconstructing the Baseline Model

Fig. 9 shows the fullStart initial model, two reconstructions of the Baseline model (Fig. 2) using synthetic travel-times based on real data from 2008-2009, and their percentage difference to the Baseline model. Both 2008-2009 reconstructions perform quite well and show more similarities to the 2009-2010 result in Fig. 8, compared to their own time window in the same figure. The main features of the Baseline model are reproduced with smeared details and diminished amplitudes. For the reconstruction without tt-errors, these maximum differences stay between ±7.0 % (Vp/Vs), ±4.5 % (Vs), and ±4.0 % (Vp). For the reconstruction using tt-errors (P: 47 ms, S: 83.7 ms), most differences stay within the same range. The small patch between 20-30 km distance has differences to the Baseline model up to +10.2 % for Vp/Vs, and +5.7 % for Vp.

Fig. 10 compares the Baseline reconstructions without tt-errors between time windows and is used to emphasize artificial differences due to the combination of regularization and differences in ray-path geometries. The panels show the percentage difference between the individual reconstructions and the 2008-2009 reconstruction. The colorbar ranges have been kept the same as in Fig. 9 for comparison. The largest differences do not reach the limits of the colorbars and large parts of the profile show close to 0 % difference between the reconstructions and the reference. This is especially the case for the 2009-2010 results, and the area between 18 and 30 km distance. The largest differences in this area occur in the periods 2012-2013 and 2013-2014. The largest differences overall occur at distances below ~18 km for periods with less seismicity (2010-2011 through to 2014-2015). The values there show strong similarities to each other during these periods (e.g. Vs has a blue band near the surface, above slightly red values, above a blue band).

Fig. 11 shows a similar comparison as Fig. 10. It compares the inversion results using real data for 2-year time windows (Fig. 8) with 2008-2009 as a reference. The colorbars are kept the same as in Figs. 9 and 10. The differences between the individual panels and the reference are much larger here, compared to the panels in Fig. 10. All time windows have values that go beyond the colorbar, indicating that these differences go beyond those between the Baseline model and the 2008-2009 reconstruction without tt-errors (Fig. 9). Even the comparison between 2009-2010 and 2008-2009 shows large differences compared to Fig. 10, even though the two time windows share an entire year of data. There are even sign inversions of the percentages, e.g. the Vp and Vs differences in the center of the profile in the years 2010-2011 through to 2015-2016 go from positive in Fig. 10 to strongly negative in Fig. 11. The changes seen in Fig. 8 therefore significantly go beyond those due to regularization effects and differences in ray-path geometries.

Next, a check for artificial differences including travel-time errors is required. Fig. 12 shows the same comparison as in Fig. 10 using Baseline reconstructions with tt-errors in the order of the root-mean-squared (RMS) misfit of the Baseline (standard deviations - P: 47 ms, S: 83.7 ms). These values represent the high end of the residuals for the individual time windows presented here. Most inversions have lower RMS misfits. In Fig. 12 the values again stay below the colorbar (Vp of 2013-2014 has a small exception), and many values stay close to 0 % difference. The biggest differences to Fig. 10 are the larger amplitude and the increased detail of the differences. Similar results were obtained when using 10 and 30 ms (for P, multiplied by 1.78 for S) for the standard deviation of the errors. The increase of the error produces larger and more detailed artificial differences. Based on Figs. 12 and 11, the differences seen in Fig. 8 significantly go beyond artificial difference due to the combined effect of travel-time errors, regularization, and ray-path geometries. This is especially true for the comparison between 2009-2010 and 2008-2009, as our results predict that a full year of common data should heavily reduce artificial differences, even with high error levels.

4. DISCUSSION

This initial investigation into the Krysuvik geothermal area provides high-resolution images up to 10 km depth using the permanent SIL-station network. A time-dependent investigation was employed to test the robustness of individual features of this “Baseline” model when using subsets of the data. This investigation shows that certain features are very robust, and that the observed changes in the results are larger than those due to differences in ray-path geometries, regularization, and data errors. The four issues regarding time-dependent seismic tomography (when using the same forward solver) have been addressed in the following manners. Differences in results due to differences in ray-path geometry were inherently reduced by using a consistent station geometry and additionally reduced through the characteristic seismicity distribution in the investigated area. The synthetic reconstructions of the Baseline model without tt-errors (Fig. 10) showed minor remaining differences between time windows (a few percent, with the maximum values obtained for the period with the least earthquakes in the area). These minor differences are due to the combination of differences in ray-path geometry and the usage of consistent regularization (only smoothing with equal factors) for inversions with different amounts of data. The comparison between the differences in the Baseline reconstruction without tt-errors and the differences seen in the results using real data thus has the following benefit. It allows us to determine if differences in models using real data go beyond differences that can be attributed to both the regularization and the ray-path geometries. As we have shown, this is the case in this study (Figs. 10-11). The final issue of data errors was investigated using different values of the standard deviation of travel-time errors in the Baseline reconstructions. The results thus investigate the combined effects of ray-path geometries, regularization, and data errors. This test showed that artificial differences produced using Gaussian distributed travel-time errors on the order of the Baseline RMS misfit were still minor compared to the changes produced using the real data (Fig. 11-12). One random set of errors cannot provide a full overview of how errors might cluster to produce high amplitudes in small regions. This clustering is unlikely the case in the results in Fig. 11, as there are large regions with big differences. These tests also do not rule out the possibility of data errors with systemic biases. To explain the remaining differences, however, these biased errors would need to have the following properties: 1) these errors would need to be quite large, 2) the systemic bias of the errors would need to change between time periods, and 3) these errors would need to be small and obscure enough to persist at the end of the work flow. Overall, errors cannot be the cause of the large differences between the results for neighboring time periods (e.g. 2008-2009 and 2009-2010, Fig. 10-12), as they have a full year of common data.

Addressing these four issues in this way only determines significant enough differences in the results in Fig. 8 to warrant rejection of the null-hypothesis, i.e. the results indicate significant changes in the subsurface. The reconstruction tests (Fig. 9) additionally show that the results of the individual time windows smooth out the heterogeneities in the Baseline model (Fig. 2) and lower the intensity of the anomalies. The results in Fig. 8 therefore have to be interpreted in light of the Baseline model, which represents a weighted average of the temporal changes. Before presenting our preliminary interpretations, we will first discuss information from literature.

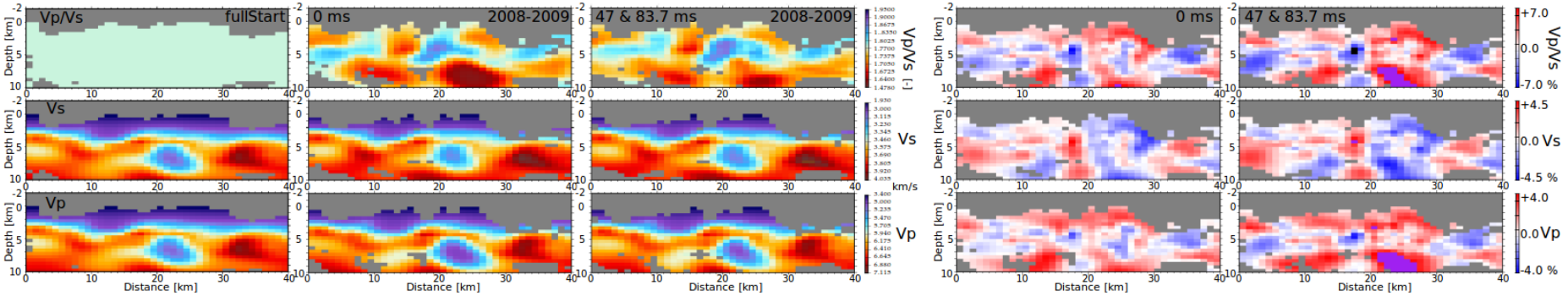

Figure 9: Left) fullStart initial model based on Baseline model. Middle) Reconstructions of the Baseline model in Fig. 2 for the period of 2008-2009 starting from the fullStart model with and without tt-errors. Right) Percentage differences between the Baseline model and these 2008-2009 reconstructions.

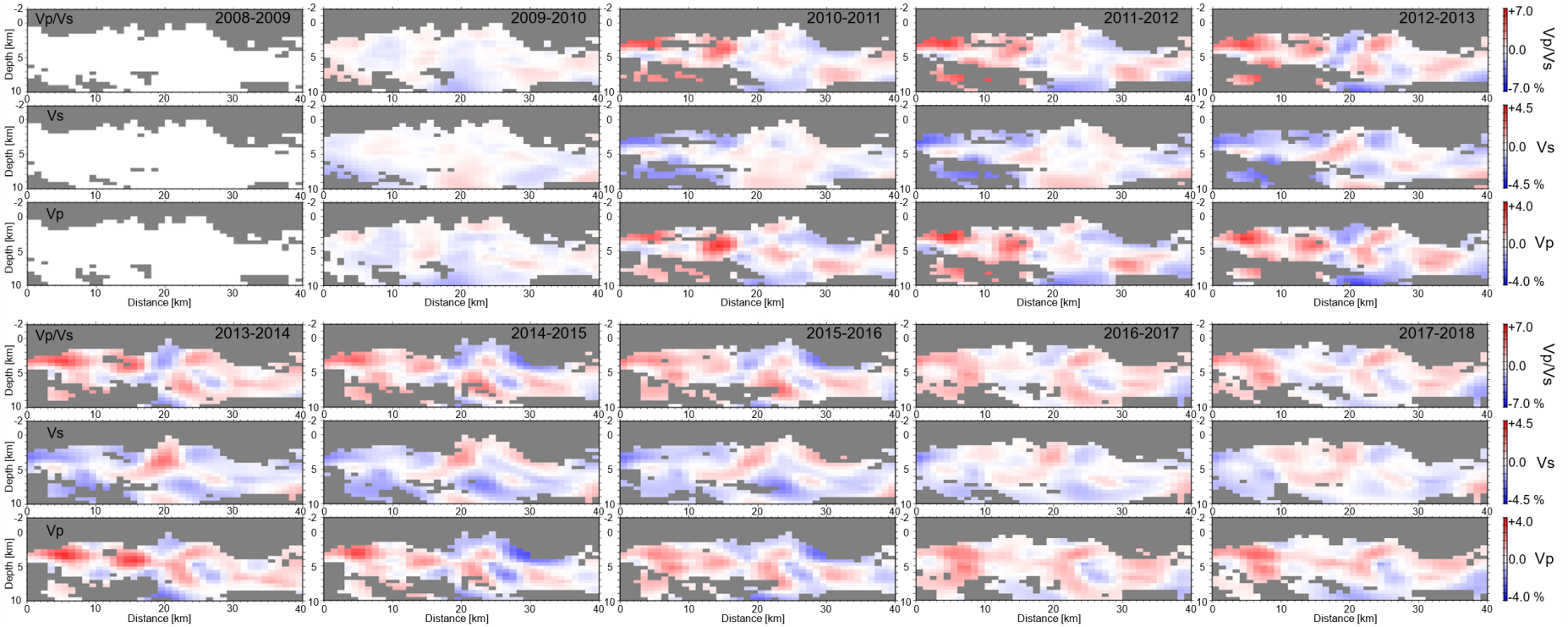

Figure 10: Comparisons between results for the reconstruction of the Baseline model without errors on the travel-times. Inversions use the fullStart initial model and 2-year time-windows. Shown are percentage differences compared to the reference result of 2008-2009. Note the difference in scale for the colorbar.

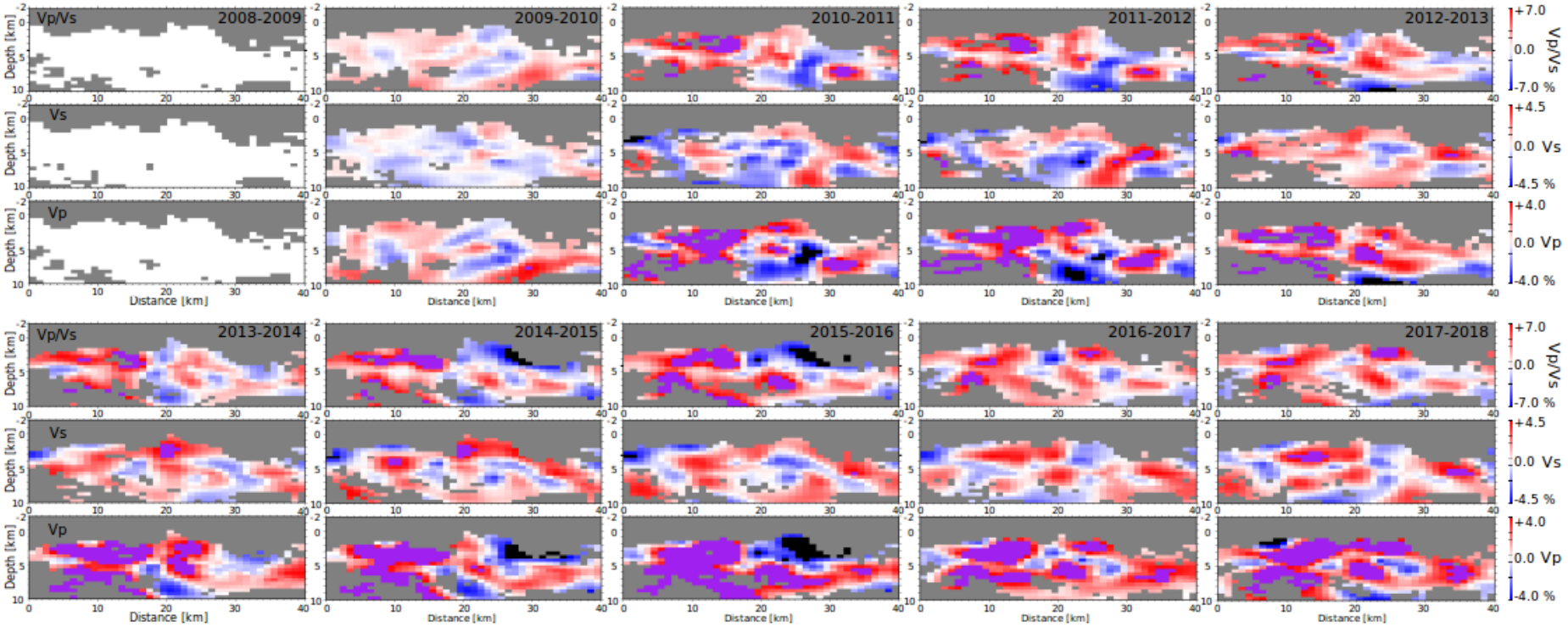

Figure 11: Comparisons between results for inversions using real data. Inversions use the fullStart initial model and 2-year time-windows. Shown are percentage differences compared to the reference results of 2008-2009. Note the difference in scale for the colorbar. Black and purple indicate values above and below the range of the colorbar, respectively.

4.1 What are we looking for?

Surface deformation can occur due to many possible sources. The signature of the observed radial surface deformation (Michalczewska et al., 2012a) could be explained magmatically with a horizontal sill, or diagonal dike (Sigmundsson et al., 2018, Fig. 11.5). Vertical sills have very different signals. A Mogi-source can also produce such a radial signal, though these have no volume. Surface deformation curves associated with magmatic replenishment of the volcanic system in the East-African Rift System (Fig. 6 in Biggs et al. 2011) are very similar to the GPS signal of the surface deformation in Krysuvik (Gudjonsdottir et al. 2018). These curves, however show shorter relaxation times in comparison, and most importantly, the uplift is permanent. Similar curves are also found in e.g. Lupi et al. (2017). These authors attribute the surface deformation at Campi Flegrei (Italy) to "Volumetric expansion of CO_2-rich fluids" below an impermeable barrier. The subsequent relaxation is then explained by this barrier fracturing and allowing the fluids to disperse. In their model, the ultimate source of these volatiles is a magma body at ~7 km depth. The time-scale of the relaxation of the surface deformation is 20 years (Fig. 1 in Lupi et al., 2017). This curve also includes a permanent vertical displacement. This work is reviewed in Troise et al. (2019), who separate the deformation effect seen at Campi Flegrei into a magmatic contribution and a hydrothermal contribution. The vertical deformation curve due to hydrothermal alteration is also quite similar to the GPS signal in Krysuvik. The relaxation time, however, lasted 30 years to reach the initial level after an uplift of more than 0.5 m. Here, adjustments to the model parameters would adjust both the uplift and relaxation time. Another study of the observations at Campi Flegrei (Rinaldi et al. 2008) obtains the most similar results to those seen in Krysuvik (Fig. 4 in Gudjonsdottir et al., 2018, with steady-state condition beforehand, Fig. 3 in Michalczewska et al., 2012b). These authors show a temporary surface deformation of 8 cm with a relaxation time of 10 years that ends with a vertical displacement below the original level, in relation with stronger degassing of a magmatic source. The results from Gudjonsdottir et al. (2018) seem to speak against the intrusion of new magmatic material into the shallow system. Their gas measurements were taken ~1.5 years after subsidence had set in and could thus have missed the main magmatic component of the gas flux. Additionally, we are unaware of what type of gas-phase signal would be produced by melting due to increased heat. If these curves are representative of their respective phenomena, then the two most likely a-priori hypotheses become the strong degassing of a magmatic source described in Rinaldi et al. (2008), and the volatiles that push up and subsequently break an impermeable barrier.

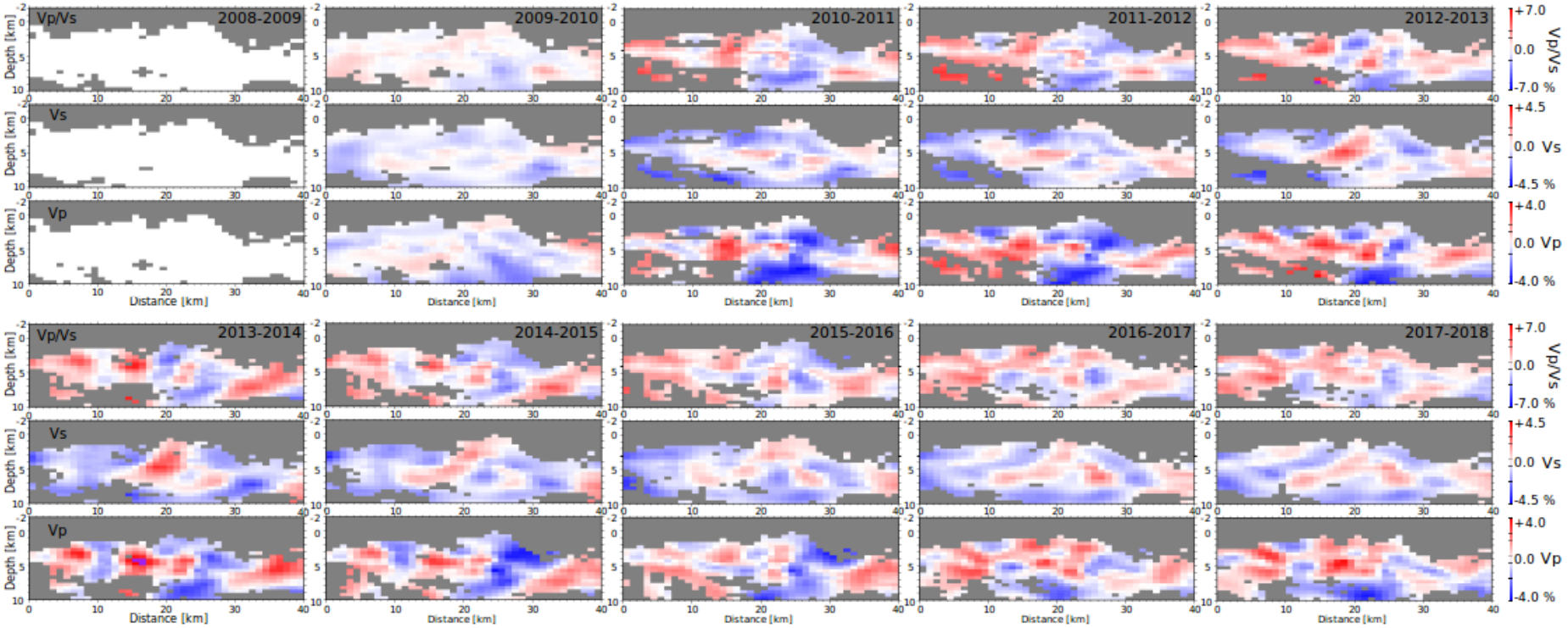

Figure 12: Comparisons between results for the reconstruction of the Baseline model using errors on the travel-times (standard deviations - P: 47 ms, S: 83.7 ms). Inversions use the fullStart initial model and 2-year time-windows. Shown are percentage differences compared to the reference result of 2008-2009. Note the difference in scale for the colorbar.

4.2 INITIAL INTERPRETATION

This initial investigation into the Krysuvik Geothermal area uses a small number of stations, compared to some of the temporary campaigns on the Reykjanes Peninsula. The permanent nature of these SIL stations allows us to set a baseline with reduced differences in ray-path geometries. A baseline which can be used for a follow-up study using a denser network which varies with time. In such a study, the distribution of the stations will result in subsurface energy being spread out to other parts of the model, similar to the effect of earthquake distributions in the current work. Such investigations using denser networks will be able to resolve smaller structures. The results would, however, need to account for the four issues with time-dependent seismic tomography, which is more difficult with a time-varying network. Comparisons between smaller campaigns would need to meet the same requirements. We therefore suggest that the baseline provided by this study would serve well to aid such comparisons, and the following initial interpretation could provide initial hypotheses to confirm or falsify. The checkerboard tests, however, do show that the resolution is good enough for the size of the features in the Baseline model (Figs. 2, and 5-7), and important features in the time-dependent results (Fig. 8). Interpreting the changes with time as changes to this average model should therefore be valid. With that disclaimer out of the way, here is our tentative interpretation of the results of this investigation.

A magmatic source would show high Vp/Vs values, low Vp and Vs values, and a lack of seismicity. Although a magma chamber would not allow an S-wave to travel through it, a volcanic plumbing system with smaller features compared to the employed parameterization could allow their propagation. The Baseline model provides several regions with these characteristics. The low-seismicity region in the west has a high Vp/Vs anomaly with a clear Vs low between ~4.5 and ~7 km depth. This may very well be the heat source for the Svartsengi power-plant. Although this feature shows up in multiple panels in Fig. 8, it is not well resolved in the checkerboard tests for this profile (Figs. 5-7), thus requiring further study. The very high Vp/Vs region centered around 18 km distance between ~3-7 km depth in the baseline could be important in the understanding of the surface deformation. It is well resolved in the Baseline and should be distinguishable in most time-dependent results. The amplitude of this feature increases during the period of inflation (2010 through to 2012) and diminishes thereafter (Fig. 8). This feature does have slightly elevated Vp values.

The hypothesis of pressurized liquid water in this region seems unlikely for two reasons. The strongly reduced seismicity, and the very high temperatures (>325°C) observed at 2 km depth (Fig. 7, Hersir et al., 2018). A better understanding of this feature would therefore require additional investigation (e.g. using the denser network). The same goes for the blue Vp/Vs feature just below (>8 km depth), which could represent an extension of the magmatic plumbing.

The low Vp/Vs anomalies in both the Baseline and time-dependent results (Figs. 2 and 8) could have multiple interpretations. This signal is produced by dry fractured rock, compressible fluids (e.g. steam, super-critical), and fractured rock containing compressible fluids. The low Vp/Vs anomaly in Fagradallsfjall (~12 km distance) is mostly associated with seismicity (e.g. 2008-2009 and 2016-2107). The top of this anomaly disappears when there is no seismicity. Fig. 7 shows that the time-dependent results should be able to resolve this difference above 6 km depth (e.g. 2014-2105). This suggests that fracturing produces this Vp/Vs low and that Vp/Vs values go back to the regional average when the fractures heal. This hypothesis is further supported by the results from Keiding et al. (2009), who suggest that seismicity in this area is mainly tectonically driven without a hydrothermal component. The Vp/Vs low between 20-30 km distance and below 5 km depth (Fig. 2) is co-located with the low Vp and Vs anomalies just below the center of inflation (e.g. Figs. 2 and 8). All three are prime candidates for the inflation source, as their top is situated at its estimated depth: ~4.5 km (Hersir et al. 2018). The robustness of the low Vp and Vs features for all time windows make them the most reliable result of this study. They are co-located with a resistive feature (~70 Ωm**)** in Hersir et al. (2018) at 5 km below see level. During the period of inflation, there is a lot of seismicity starting within these anomalies (> 6 km depth) and reaching up to ~1 km depth near the inflation center. Where the Vp/Vs values are low, this clearly indicates a super-critical reservoir. The time-dependent results in 2009-2010 through to 2011-2012 (Fig. 8) suggest that some of the compressible fluids escaped towards the surface. This low Vp/Vs "plume" has stronger amplitudes where there is seismicity and still occurs where the seismicity is greatly reduced. This is likely explained by compressible fluids with and without fractures.

Therefore, our results support both hypotheses: magma degassing, and fluids expanding below and breaking an impermeable barrier. Although our results do give more credence to the latter, we suggest both are possible simultaneously based on our results and a few details in Fig. 4 in Gudjonsdottir et al. (2018). After the seismic swarm at the beginning of 2011, uplift continued and seemed to level off until the beginning of 2012. At that time, a downwards vertical shift is seen in the vertical displacement accompanied by a small jump in the cumulative seismic moment. This shift marks the onset of the subsidence in the area. This suggests that this was the moment when the impermeable barrier broke. Infiltration of a dike into the shallow system is unlikely, as no permanent surface deformation was observed, next to the arguments made by Gudjonsdottir et al. (2018). Increased degassing from a deeper source could explain the differences at depth between the panels 2008-2009 and 2009-2010 in Fig 8. It could also explain part of the origin of the super-critical reservoir. This aspect would need further investigation (e.g. using the denser network).

5. CONCLUSIONS

Using the permanent SIL-station geometry, with 15 years of earthquake data (2004-2018), this investigation produced subsurface images of the Krysuvik geothermal area with high resolution up to 10 km depth. The robustness of individual features in this "Baseline" model was investigated using time-dependent seismic tomography. This investigation was able to show significant changes with time on the time scale of the observed surface deformation. This was accomplished by systematically overcoming the four issues associated with time-dependent seismic tomography, which can bias results of individual time-windows. These are: 1) temporal differences in earthquake distributions, 2) temporal differences in station geometries, 3) errors e.g. in the arrival times, and 4) the impact of regularization when using different amounts of earthquakes, and P- and S-wave travel times. The features of the Baseline model and changes to it have been discussed in light of the appraisal information. Based on this, several hypotheses were set up. After integrating the results of this study with available information from literature, we conclude that the most likely scenarios to explain the observed surface deformation in Krysuvik are: 1) strong degassing of an existing magmatic source, and 2) uplifting of an impermeable barrier by expanding fluids, followed by relaxation of the system after the barrier fails through fracturing. A combination of both is also plausible based on the seismic images. The lack of permanent uplift combined with other arguments from literature make magmatic infiltration into the shallow system unlikely. There are indications of magmatic infiltration near 10 km depth, which will need further investigation. We interpret the features of the model as indicative of dehydration of minerals at greater depth, combined with smeared out features of the magmatic plumbing of this volcanic system. These results can be used as a baseline for a follow-up study using a denser network which varies with time. Although the resolution of these results are limited compared to such a denser network, the most robust feature is already delineated very clearly. The results predict a large super-critical reservoir below ~5 km depth, which would serve well as a heat and fluid source for a new power plant.

6. ACKNOWLEDGEMENTS

The authors would like to thank Halldór Geirsson, who pointed out the estimated inflation center in the GPS results of Michalczewska et al. (2012a), and explained the difference of the GPS results to those using INSAR images of Michalczewska et al. (2012b). This work was supported by the Swedish strategic research programme StandUp for Energy.

REFERENCES

Benz, H.M., Chouet, B.A., Dawson, P.B., Lahr, J.C., Page, R.A., and Hole, J.A.: Three-dimensional P- and S-wave velocity structure of Redoubt Volcano, Alaska, *J. Geophys. Res.*, **101(B4)**, (1996), 8111-8128.

Biggs, J., Bastow, I.D., Keir, D., and Lewi, E.: Pulses of deformation reveal frequently recurring shallow magmatic activity beneath the Main Ethiopian Rift, *Geochemistry, Geophysics, Geosystems*, **12(9)**, (2011).

Einarsson, P. (2008). Plate boundaries, rifts and transforms in Iceland. *Jökull*, **58(12),** 35-58.

Flovenz, O.G., and Gunnarsson, K.: Seismic crustal structure in Iceland and surrounding area, *Tectonophysics*, **189(1-4)**, (1991).

Fridleifsson, G.O., Elders, W.A., Zierenberg, R.A., Stefansson, A., Fowler, A.P., Weisenberger, T.B., ... and Mesfin, K.G.: The Iceland Deep Drilling Project 4.5 km deep well, IDDP-2, in the seawater-recharged Reykjanes geothermal field in SW Iceland has successfully reached its supercritical target. *Scientific Drilling*, **23**, (2017), 1-12.

Gallardo, L.A., and Meju, M.A.: Joint two-dimensional DC-resistivity and seismic travel-time inversion with cross-gradients constraints, *J. Geophys. Res.*, **109,** (2004), B0331.

Geoffroy, L., and Dorbath, C.: Deep downward fluid percolation driven by localized crust dilatation in Iceland. Geophysical research letters, **35(17)**, (2008).

Gudjonsdottir, S.R., Ilyinskaya, E., Hreinsdottir, S., Bergsson, B., Pfeffer, M.A., ... and Oladottir, A.A.: Gas emissions and crustal deformation from the Krysuvik high temperature geothermal system, Iceland. J. Volcanol. Geotherm. Res., (2018).

Hersir, G.P., Arnason, K., Vilhjalmsson, A.M., Saemundsson, K., Agustsdottir, P., and Fridleifsson, G.A.: Krysuvik high temperature geothermal area in SW Iceland: geological setting and 3D inversion of magnetotelluric (MT) resistivity data, J. Volcanol. Geotherm. Res., (2018).

Hole, J.A.: Nonlinear high-resolution three-dimensional seismic travel time tomography, *J. Geophys. Res.*, **97**, (1992), 6553-6562.

Hreinsdottir, S., and Michalczewska, K.:URL: https://strokkur.raunvis.hi.is/~sigrun/KRIV.html, accessed 29.07.2019.

Julian, B.R., and Foulger, G.R.: Time-dependent seismic tomography. *Geophys. J. Int*., **182(3)**, (2010), 1327-1338.

Keiding, M., Lund, B., and Arnadottir, T.: Earthquakes, stress, and strain along an obliquely divergent plate boundary: Reykjanes Peninsula, southwest Iceland, *J. Geophys. Res.: Solid Earth*, **114(B9)**, (2009).

Koulakov, I., Gordeev, E.I., Dobretsov, N.L., Vernikovsky, V.A., Senyukov, S., Jakovlev, A., and Jaxybulatov, K.: Rapid changes in magma storage beneath the Klyuchevskoy group of volcanoes inferred from time-dependent seismic tomography, *J. Volcanol. Geotherm. Res.*, **263**, (2013), 75-91.

Landsvrikjun: https://www.landsvirkjun.com/researchdevelopment/submarinecabletoeurope, accessed 23.12.2019

Lupi, M., Frehner, M., Weis, P., Skelton, A., Saenger, E.H., Tisato, N., ... and Driesner, T.: Regional earthquakes followed by delayed ground uplifts at Campi Flegrei Caldera, Italy: Arguments for a causal link, *Earth Planet. Sci. Lett.*, **474**, (2017), 436-446.

Michalczewska, K., Hreinsdottir, S., Arnadottir, Th., Hjaltadottir, S., Agustsdottir, Th., and Geirsson, H.: Crustal deformation in the Krisuvik area. *Proceedings,* Spring meeting of the Iceland Geoscience Society. Abstract volume, (2012). p. 51. (cited as 2012a)

Michalczewska, K., Hreinsdottir, S., Arnadottir, Th., Hjaltadottir, S., Agustsdottir, Th., Gudmundsson, M.T., Geirsson, H., Sigmundsson, F., and Gudmundsson, G.B.: The inflation and deflation episodes in the Krisuvik volcanic system, *Proceedings,* AGU Fall Meeting, December 2012. Abstract ID: V33A-2843. (cited as 2012b)

Paige, C.C., and Saunders, M.A.: LSQR: An algorithm for sparse linear equation and sparse least square. *ACM. Trans. Mathematical Software*, **8**, (1982), 43-71.

Podvin, P., and Lecomte, I.: Finite difference computation of traveltimes in very contrasted velocity models: a massively parallel approach and its associated tools. *Geophys. J. Int.*, 105(1), (1991), 271-284.

Rinaldi, A.P., Todesco, M., and Bonafede, M.: Hydrothermal instability and ground displacement at the Campi Flegrei caldera. *Phys. Earth Planet. In.*, **178.3-4**, (2010), 155-161.

Sasaki, D., and Nakayama, M.: Risk management in an electricity transmission project between Iceland and the UK. *Int'l J. Soc. Sci. Stud.*, **4**, (2016b), 17.

Sigmundsson, F., Parks, M., Pedersen, R., Jonsdottir, K., Ofeigsson, B.G., Grapenthin, R., ... and Hjartardottir, A.R.: Magma movements in volcanic plumbing systems and their associated ground deformation and seismic patterns. *In Volcanic and Igneous Plumbing Systems*, (2018), 285-322, Elsevier.

Troise, C., De Natale, G., Schiavone, R., Somma, R., and Moretti, R.: The Campi Flegrei caldera unrest: Discriminating magma intrusions from hydrothermal effects and implications for possible evolution, *Earth-science reviews,* (2018).

Tryggvason, A., Rögnvaldsson, S.Th., and Flovenz, O.G.: Three-dimensional imaging of the P- and S-wave velocity structure and earthquake locations beneath Southwest Iceland, *Geophys. J. Int.*, **151**, (2002), 848-866

Tryggvason, A., and Bergman B.: A traveltime reciprocity discrepancy in the Podvin and Lecomte time3d finite difference algorithm, *Geophys. J. Int.*, **165(2)**, (2006), 432-435.

Tryggvason, A., and Linde, N.: Local earthquake (LE) tomography with joint inversion for P- and S-wave velocities using structural constraints. Geophys. Res. Lett., **33**, (2006), L07303.

Weir, N.R., White, R.S., Brandsdottir, B., Einarsson, P., Shimamura, H., and Shiobara, H.: Crustal structure of the northern Reykjanes Ridge and Reykjanes Peninsula, southwest Iceland. *J. Geophys. Res.: Solid Earth*, **106(B4)**, (2001), 6347-6368.